Journal of Materials Chemistry A

Accepted Manuscript

ROYAL SOCIETY OF CHEMISTRY

www.rsc.org/materialsA

Journal of Materials Chemistry A RSCPublishing

ARTICLE

Cysteine-containing oligopeptide β-sheets as redispersants for agglomerated metal nanoparticles

Cite this: DOI: 10.1039/x0xx00000x

Received 00th March 2015,
Accepted 00th March 2015

DOI: 10.1039/x0xx00000x

www.rsc.org/

Tsukasa Mizutaru,[a] Taro Sakuraba,[a] Toru Nakayama,[a] Galina Marzun,[b] Philipp Wagener,[b] Christoph Rehbock,[b] Stephan Barcikowski,[b] Katsuhisa Murakami,[c,d] Junichi Fujita,[c,d] Noriyuki Ishii[e] and Yohei Yamamoto*[a,d]

Oligopeptide β-sheets comprising fluorenyl methoxy carbonyl (Fmoc) group on its N-terminus and five amino acid residues of cysteine, lysine and valine displays redispersive properties of agglomerated metal nanoparticles (MNPs, M = Au, Cu, Pt and Pd). The ligand-free MNPs prepared by laser ablation technique in liquid keep high dispersion state due to the inherent surface charges delivered by anionic species present in solution but may agglomerate after the preparation which depends on concentration or salinity. We show how the agglomerated MNPs can be returned to the dispersive state by adding the Fmoc-oligopeptide β-sheets in methanol, which is characterized by photoabsorption spectroscopy and transmission electron microscopy. Systematic studies varying the concentration, the amino acid sequences and secondary structures of a series of the oligopeptides clarify that the β-sheet structure is essential for the redispersion of the MNPs, where metal-binding thiol groups are integrated on one side and positively charged amino groups are located on the other side of the β-sheet. A possible mechanism for the redispersion may be that the agglomerated MNPs are subsequently enwrapped by the flexible β-sheets and gradually separated due to the reconstruction of peptide β-sheets under the assembly/disassembly equilibrium.

1. Introduction

Metal nanoparticles (MNPs) are widely utilized as catalysts and photocatalysts,[1] additives for solar cells[2] and as materials for chemical and biological sensing[3] due to their unordinary electronic and plasmonic states. Fabrication procedures of MNPs include liquid-, gas- and solid-phase processes.[4] The morphology of the MNPs is generally retained when they are immobilized on a solid surface or in a supported medium. On the other hand, agglomeration of MNPs often takes place in solution. The agglomeration suppresses their plasmonic characters, which is disadvantageous for utilizing MNPs as tools for plasmonic sensing. In addition, a well-dispersed stable colloid is a key requirement for a diversity of other applications such as biomedicine,[5] toxicology studies[6] or catalysis.[7]

Especially, when the nanoparticles are small, the high surface energy of the particles can cause agglomeration. As the size of the particles decreases, the interaction forces between particles increases, resulting in a loss of their specific properties. Furthermore, once the agglomeration occurs, it is rather difficult to redisperse nanoparticles to their original dispersive state.[8]

Ligand free MNPs in aqueous or organic solvents can be produced by pulsed laser ablation in liquids.[9] Irradiation of a focused high energy density laser beam to a metal target in a solvent results in a production of highly dispersed MNPs with several to several tens of nanometres. Because the resulting MNPs are charged and covered on their surfaces with anionic species that are present in solution, a repulsive electrostatic force takes place between the particles. Accordingly, the MNPs maintain their highly dispersed colloidal state in solutions of micromolar salinity and at moderate particle concentrations.[9] However, in pure solvents or at high concentrations, the stability of the dispersed MNPs gradually diminishes and several months after the preparation of the colloidal solution, agglomeration of the MNPs might occur. In such cases, the plasmonic characters of the MNPs are altered due to plasmon coupling, inducing a red shift of the surface plasmon resonance (SPR) band and an increased scattering in the near infrared (NIR) spectral regime.[10] Therefore, if the agglomerated MNPs can be redispersed efficiently, the plasmonic property will be recovered to the original state, and the MNPs can be utilized as renewable materials, which is beneficial from an ecological and sustainable point of view.

Redispersion may be done via ultrasonification in a solvent, where the liquid is oscillating due to the energy transfer and causes nucleation and collapse of solvent bubbles. Then agglomerates can be broken due to the bubble collapse on the solid surfaces. Deagglomeration is then influenced by the input energy and time. However, reagglomeration can take place in

case the particles are not sufficiently stabilized. Furthermore abrasion of the ultrasonic horn can occur, which may cause unwanted contaminations.

In this study, we developed redispersants for agglomerated MNPs, and found that a short oligopeptide with a certain amino acid sequence can redisperse them very efficiently. The secondary structure of the oligopeptides (β-sheet structure) plays an important role for the redispersion of MNPs. When peptides form β-sheet, the side chains of amino acids protrude alternately on the upper and lower sides of the β-sheet.[11] The redispersive oligopeptides include one cysteine (C) and one lysine (K) residue. Cysteine has a thiol side chain that tends to bind with metals, while lysine has an amino group on the side chain which is positively charged in a neutral aqueous solution. As a result of the β-sheet formation, metal-binding with thiol side chains predominantly occurs on one side of the β-sheet, while the positive charges are located on the other side. These bilateral properties of the peptide β-sheet may be responsible for re-dispersing agglomerated MNPs. A fluorenyl methoxy carbonyl (Fmoc) group attached on the N-terminus of the oligopeptides plays a role of facilitating the β-sheet formation of the peptide.

2. Experimental

2.1. Synthesis and characterization of oligopeptides

Oligopeptides are synthesized with a typical Fmoc-solid phase peptide synthesis technique with the following three protocols; [i] *Fmoc deprotection*, [ii] *Loading of Fmoc-amino acid monomer*, and [iii] *Cleavage from the resin*, as reported previously.[11]

[i] *Fmoc deprotection*: Typically, piperidine (2 mL) was added to a dimethylformamide (DMF, 8 mL) suspension of Fmoc-SAL resin (0.55 mmol g^{-1}, 0.5 g, Watanabe Chemical Co.), and the mixture was stirred for 20 min at 25 °C. The solution was removed by filtration and the resin was washed ten times with DMF (3 mL, 1 min stirring).

[ii] *Loading of Fmoc-amino acid monomer*: Typically, to the resin subjected to protocol [i] were added Fmoc-amino acid monomer (Fmoc-Lys(Trt)-OH, Fmoc-Cys(Trt)-OH, Fmoc-Val-OH, Fmoc-Glu(Trt)-OH, or Fmoc-His(Trt)-OH, 1.1 mmol), HBTU (375 mg, 0.99 mmol), HOBT (148 mg, 1.1 mmol), DMF (10 mL), and DIPEA (385 μL, 2.2 mmol) in this order, and the mixture was stirred for 1 h. The solution was removed by filtration and the resin was washed ten times with DMF. The procedures [i] and [ii] are repeated for preparation of resin bearing Fmoc-oligopeptides. For the preparation of H-oligopeptide, the procedure [i] is repeated one more time.

[iii] *Cleavage from the resin*: Typically, the resin bearing the R-oligopeptide (R = Fmoc or H) was washed three times with Et_2O (3 mL, 5 min stirring), dried under vacuum. To the resin was added a mixture of CF_3CO_2H (TFA, 2.85 mL), Et_3SiH (0.075 mL), and H_2O (0.075 mL), and the mixture was stirred for 2 h at 25 °C. The mixed solution of the resin was washed alternately with MeOH (3 mL, 3 min stirring) and CH_2Cl_2 (3 mL, 3 min stirring) three times. The solution was evaporated to dryness, and the residue was purified by reprecipitation with MeOH/Et_2O at least three times, affording desired R-oligopeptide as white powdery substance with 20–40% yield.

The products were subjected to recycling preparative HPLC (Japan Analytical Industry model LC-9210 II NEXT recycling preparative HPLC equipped with a JAIGEL-ODS-AP-A column) with MeOH/TFA (100/0.1) as an eluent, where the major fraction was collected and evaporated to allow isolation of the corresponding R-oligopeptide as white solid. The final products were characterized by MALDI-TOF MS spectrometry on an AB SCIEX model TOF/TOF(TM) 5800 system spectrometer using CHCA as a matrix. The synthesized Fmoc-peptide, for example, Fmoc-VKVVC as representative, is soluble in MeOH, EtOH and dimethyl sulfoxide, while solubility in water, acetone and chloroform is low.

2.2. Self-assembly of oligopeptides and characterization of the secondary structure

A given amount of oligopeptide was dissolved in MeOH (0.5 mM), and the resultant solution was kept at 25 °C for 7 days in the dark. The secondary structures were evaluated by circular dichroism (CD) spectroscopy, X-ray diffraction (XRD), attenuated total reflection (ATR) Fourier transform infrared (FT-IR) spectroscopy, and transmission electron microscopy (TEM). CD spectra in MeOH (0.5 mM) were recorded at 25 °C with a JASCO model J-1000 spectropolarimeter using a 1-mm path length SQ-grade quartz cell. ATR FT-IR Spectra were recorded at 25 °C with a JASCO model FT/IR-4200 Fourier transform infrared spectrometer equipped with a model PR0450-S ATR attachment. For sample preparation, two drops of a MeOH suspension containing oligopeptide (0.5 mM) were put onto ATR sample stage and air-dried. XRD patterns were recorded at 25 °C on a Rigaku model MiniFlex600 X-ray diffractometer with a Cu$K\alpha$ radiation source (λ = 1.5406 Å, 40 kV, 15 mA, scan speed: 0.2° min^{-1}) equipped with model D/Tex Ultra2-MF high-speed 1D detector. All the diffraction patterns were obtained with a 0.01° step in 2θ. TEM image of self-assembled Fmoc-VKVVC were recorded on a FEI Tecnai F20 transmission electron microscope operating the accelerating voltage at 120 kV. For sample preparation, a dispersion of the self-assembled sample (~5 μL) was drop-cast onto a specimen grid covered with a thin carbon support film, which was hydrophilized by glow discharge. Images were recorded on a Gatan slow scan CCD camera (Retractable Multiscan Camera) under low dose conditions. TEM of AuNPs and those mixed with self-assembled Fmoc-VKVVC were recorded on JEOL model JEM-2100 transmission electron microscope operating the accelerating voltage at 200 kV. For preparation, sample dispersions were drop-cast onto a 200 mesh Cu grid covered with a carbon grid (Nisshin EM), which was hydrophilized by oxygen plasma for 30 s with 100 W (Yamato model PR500 plasma reactor). The sample was air-dried overnight in atmosphere.

Photoluminescence (PL) spectra were measured at 25 °C with a JASCO model FP-6500 spectrofluorometer. For sample preparation, MeOH solutions of tris(8-hydroxyquinoline)aluminum (Alq_3, 0.22 mM, 1 mL) and its mixture with self-assembled Fmoc-VKVVC in MeOH (0.5 mM, total amount of 1 mL) were added to aqueous solutions of AuNPs (1 mL). A 10-mm path length quartz cuvette was used for PL measurements with the excitation wavelength, excitation and emission band widths, response and sensitivity factors set at 390 nm, 3 nm, 3 nm, 0.02 sec and medium, respectively. The scan rate and the number of integration were 2000 nm min^{-1} and 10, respectively. In addition, MeOH/water mixed solution of Alq_3 was prepared and measured as a control.

For propensity calculation of the β-sheet formation, TANGO algorithm program was utilized, which was freely downloaded via internet at http://tango.embl.de/.[12] The

calculation was carried out under the following conditions; pH = 8.5, T = 298.15 K, and ionic strength = 0.004.

2.3. Preparation of metal nanoparticle and redispersion with peptides

Aqueous and organic solvent dispersions of MNPs were prepared according to the reported procedure.[9] Laser generation of surfactant-free metal nanoparticles was carried out using a picosecond Nd:YAG laser (Ekspla Atlantic 1064/532) with 9.8 ps pulse duration and at a repetition rate of 100 kHz. A metal target (Au 99.99% Alfa Aesar, Cu 99.95% Goodfellow, Pt 99.99% Alfa Aesar, and Pd 99.95% Alfa Aesar) was placed in a self-constructed batch reactor made of Teflon.[9c,9j] The reactor was filled with 30 mL solvent and the target was irradiated at a fundamental wavelength of 1064 nm with laser pulse energy of 126 μJ. During the laser ablation, the focused laser beam was spirally scanned on the target with a scanner optic, which allows an increasing productivity due to a temporal and spatial bypassing of the cavitation bubble. The concentrations of the MNPs were determined by weighing the targets before and after ablation with a microbalance (PESA Weighing Systems). The concentration values were 55.2 μg mL^{-1} for AuNPs in water, 21.4 μg mL^{-1} for CuNPs in acetone, 47.6 μg mL^{-1} for PtNPs in 0.1 mM NaOH aqueous solution and 96.7 μg mL^{-1} for PdNPs in 0.2 mM NaOH aqueous solution.

For redispersion experiments, MeOH solutions of oligopeptides (0.5 mM), which had been incubated for 7 days, were added to the MNP dispersion (1/1 v/v). At this peptide concentration, the amount of added molecules per nanoparticles is about 407, which correspond to ~1 Peptide per surface atom assuming an average particle size of 5 nm. The mixtures were kept for 3 days in dark in order to avoid the effect of light. The redispersion experiments using MeOH solution of 1-dodecanethiol ($C_{12}H_{25}SH$) (0.5 mM) were carried out in the same way. Electronic photoabsorption spectra were recorded on a JASCO model UV-650 UV-vis-NIR spectrophotometer within a wavelength range of 300–900 nm.

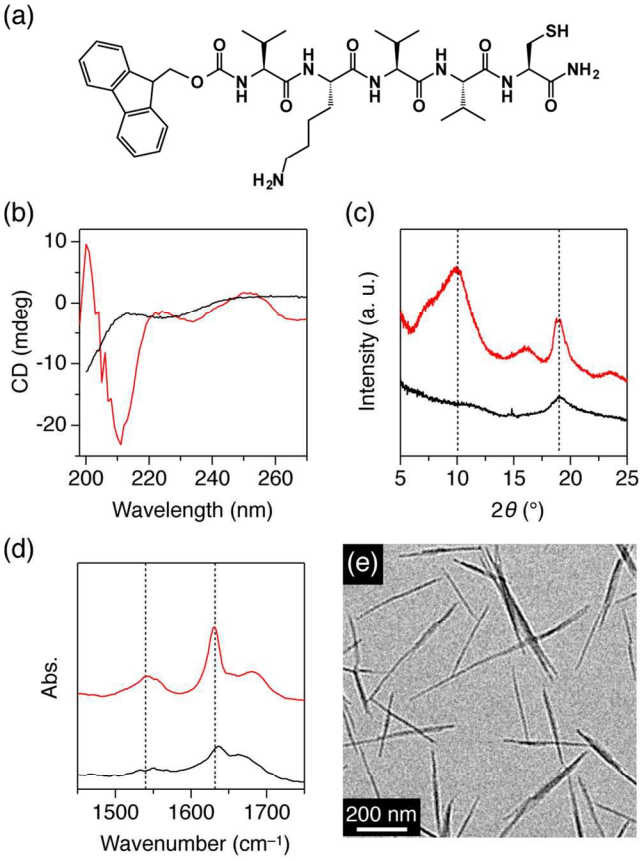

Fig. 1. (a) Molecular structure of R-VKVVC (R = Fmoc). CD spectra in MeOH (b), XRD patterns (c) and FT-IR spectra of self-assembled Fmoc-VKVVC (red) and H-VKVVC (black). The dotted lines in (c) indicates 2θ angle of 10 and 18°, while that in (d) indicate wavenumbers of 1540 and 1630 cm^{-1}. (e) TEM micrograph of Fmoc-VKVVC self-assembled in MeOH.

3. Results

3.1. Amino acid sequences and propensity for β-sheet formation

In advance to the peptide synthesis, the propensity for β-sheet formation was simulated by TANGO algorithm program.[12] For the formation of β-sheets with thiol side chains of C on one side and one amino side chain of K on the other side, the following two conditions are adopted. [1] The total number of the amino acid residues is set on odd in order to obtain such side chain configuration for β-sheets with both parallel and antiparallel conformations. In this study, five amino acid residues (pentapeptide) are adopted. [2] One C and one K are located on odd- and even-numbered amino acid sequence, respectively, and three valines (V) are occupied in the remaining sites. Among the possible amino acid sequences satisfying these conditions, VKVVC shows the highest total TANGO score (66.2). We synthesized Fmoc-substituted VKVVC (Fig. 1a), and its deprotected form, H-VKVVC, by the solid phase synthesis. As a control, Fmoc-KVVC, Fmoc-VVC, Fmoc-VC and Fmoc-C, where the number of amino acid residues in Fmoc-VKVVC was reduced one by one from the N-terminus, and Fmoc-KC without V residues were synthesized. Fmoc-pentapeptides with different sequences, Fmoc-VVVKC, Fmoc-VVVVC (without K residue), Fmoc-VKVVE and Fmoc-VKVVH (glutamic acid E, and histidine H, instead of C) were also synthesized for comparison.

□□□□□β-Sheet formation properties of pentapeptides

At first, self-assembling features of R-VKVVC (R = Fmoc, H, Fig. 1a) were investigated. Figure 1b shows CD spectra of R-VKVVC in MeOH (0.5 mM). H-VKVVC displayed a negative ellipticity at around 200 nm. On the other hand, the spectrum of Fmoc-VKVVC showed negative ellipticity at ~210 nm, and the elipticity turned to positive at 200 nm. This contrastive behaviour indicates that H-VKVVC assembles randomly in MeOH, while Fmoc-VKVVC adopts □β-sheet conformation.[11c,13] Powder XRD pattern of Fmoc-VKVVC showed strong diffraction peaks at 2θ = 10 and 18° (d = 8.8 and 4.7 Å, respectively), which were attributed to the intersheet and interstrand distances of the peptide□β-sheets (Fig. 1c, red).[11c,14] FT-IR spectrum of Fmoc-VKVVC also showed evidence of β-sheet structure, where strong amide I and II bands were observed at 1630 and 1540 cm^{-1}, respectively (Fig. 1d, red).[13] On the other hand, H-VKVVC hardly showed such evidences of the β-sheet formation in XRD and FT-IR spectroscopy (Fig. 1c and d, black).

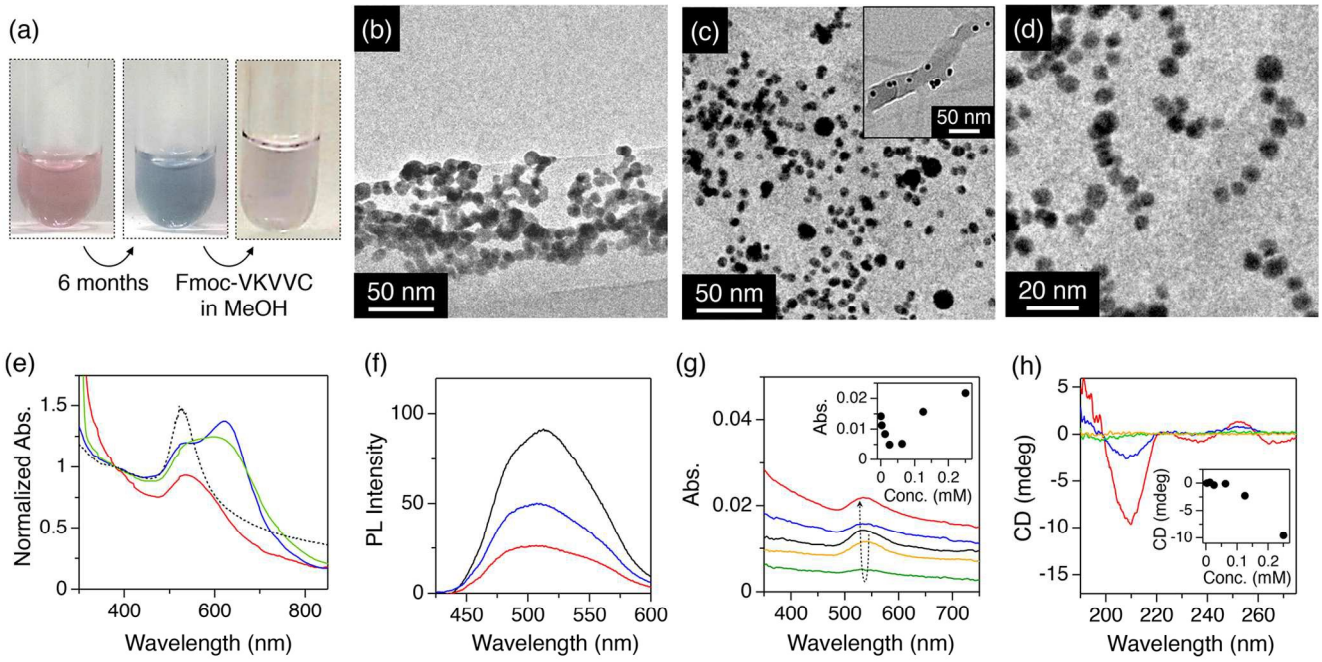

Fig. 2. (a) Photographs of the aqueous dispersion of AuNPs just after preparation (left), that 6 months after the preparation (centre) and that 6-months after the preparation, addition of MeOH solution of self-assembled Fmoc-VKVVC and then aged for 3 days (right). (b) TEM micrograph of agglomerated AuNPs in water. (c, d) TEM micrographs of agglomerated AuNPs after addition of MeOH solution containing Fmoc-VKVVC. (e) Electronic photoabsorption spectra of as-prepared AuNPs in water (dotted), agglomerated AuNPs in water (blue), and after addition of MeOH solution of Fmoc-C (green) and Fmoc-VKVVC (red) into the agglomerated AuNPs in water. The spectra were normalized by the interband absorption at 380 nm, where the absorbance is not influenced by the agglomerated state but proportional to gold mass.[9d] (f) Photoemission spectra of MeOH/water (1/1 v/v) mixed solution of Alq_3 (black), mixture of Alq_3 and agglomerated AuNPs (blue), and Alq_3 and AuNPs redispersed by self-assembled Fmoc-VKVVC (red). (g) Electronic photoabsorption spectra of agglomerated AuNPs (black) and that mixed with Fmoc-VKVVC in MeOH. Total concentrations of Fmoc-VKVVC in MeOH/water (1/1 v/v): 0.0025 (orange), 0.0625 (green), 0.125 (blue) and 0.25 mM (red). Inset shows plot of absorbance at 530 nm versus total concentration of Fmoc-VKVVC. (h) CD spectra of Fmoc-VKVVC in MeOH/water (1/1 v/v). Total concentrations of Fmoc-VKVVC: 0.0025 (orange), 0.0625 (green), 0.125 (blue) and 0.25 mM (red). Inset shows plot of CD intensity at 210 nm versus total concentration of Fmoc-VKVVC.

TEM micrograph of Fmoc-VKVVC, self-assembled in MeOH, displayed nanofibrillar structures with 10–30 nm width and sub-micrometer length (Fig. 1e). Such fibrillar morphology is typical of peptide β-sheet. Considering the amino acid sequence and previous reports on assembly of Fmoc-substituted oligopeptides,[15] the β-sheet most likely adopts antiparallel configuration, where the side chains of K (animo group) and C (thiol group) located separately on upper and lower sides of the β-sheet, respectively.

3.3. Redispersion of MNPs with cysteine-containing peptides

Next, redispersion properties of the peptides for agglomerated MNPs were investigated. The as-prepared aqueous solution of highly dispersed AuNPs was coloured pink (Fig. 2a, left) due to the plasmon absorption at about 530 nm (Fig. 2e, dotted). However, the colour of the solution changed to blue 6 months after preparation (Fig. 2a, centre), indicating that AuNPs became agglomerated. In fact, TEM micrograph showed that the AuNPs after 6 months are heavily agglomerated and fused with one another (Fig. 2b).

When the MeOH solution of the β-sheets of Fmoc-VKVVC (0.5 mM) was added to the aqueous dispersion of the agglomerated AuNPs and the mixture was aged for 3 days, the colour of the dispersion gradually turned back to pink (Fig. 2a, right), which is analogous to the initial state of the AuNP dispersion in water. Electronic photoabsorption spectroscopy showed apparent spectral change before and after addition of the MeOH solution of Fmoc-VKVVC. Before addition, the absorption maximum appeared at 630 nm with an absorption shoulder at 530 nm (Fig. 2e, blue). After addition, the peak at 630 nm completely disappeared, and absorption at 530 nm due to the surface plasmon resonance of isolated AuNPs was observed (Fig. 2e, red). TEM micrographs after addition of Fmoc-VKVVC showed that each AuNP is clearly separated from its neighbouring particle with a certain distance of 1–5 nm (Fig. 2c and d). The presence of the underlying peptides may not be detectable due to the relatively weak electron beam scattering of organic matter in comparison to heavy elements like Au. However, in the wide range view, we can identify that dispersed AuNPs are attached separately on β-sheets (Fig. 2c, inset). The pink colour of the dispersion was maintained at least 9 months after addition of MeOH solution of Fmoc-VKVVC.

AuNPs can act as a quencher for the fluorescence of dyes.[16] This phenomenon is observed in systems where the dye serves as the donor and the plasmonic NP as the acceptor species. It is predominantly attributed to two separate effects. Firstly, non-radiative energy transfer similar to FRET is found, however a second radiative effect, originating from an out of phase oscillation of fluorophores and metal NP, was also observed.[17]

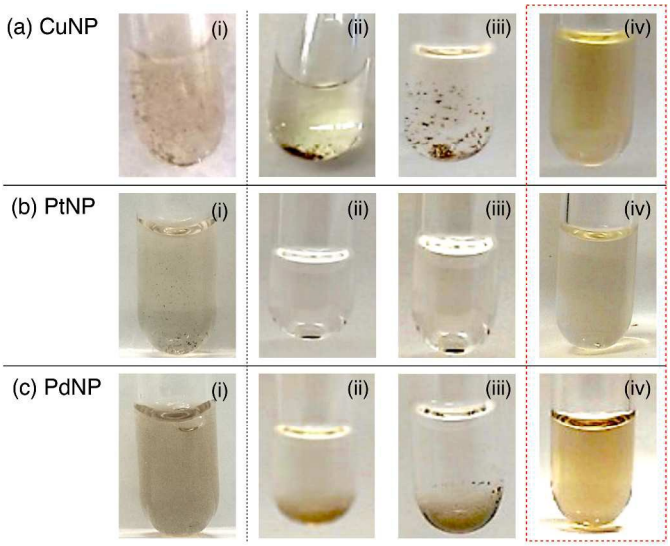

Fig. 3. Photographs of dispersions of CuNPs (a), PtNPs (b) and PdNPs (c) 6 months after preparation (i) and after addition of MeOH (ii), MeOH solution of Fmoc-C (iii) and MeOH solution of Fmoc-VKVVC (iv).

Consequently, efficient fluorescence quenching by metal NP may also occur where the spectral overlap between fluorescence emission and NP absorbance is relatively small, e.g., in case of the combination of AuNP and red emitting dyes like Cy5.[17b] In both cases, the fluorescence quenching effect is enhanced significantly when the distance between fluorophore and NP surface is decreased as well as when the particle size is increased.[17b]

We investigated the fluorescence quenching properties of the redispersed AuNPs. A MeOH/water mixed solution of Alq_3 shows a PL band centered at 510 nm (Fig. 2f, black), which overlaps well with plasmon absorption band of AuNPs (~530 nm). Accordingly, fluorescence quenching by non-radiative effects is prone to occur in the observed system. In fact, 69% of the fluorescence from Alq_3 was quenched when the AuNPs, redispersed by the β-sheets of Fmoc-VKVVC, were added to a solution containing Alq_3 (Fig. 2f, red). The degree of quenching is much higher than in case of the original partially agglomerated AuNP, where quenching of ~46% was observed (Fig. 2f, blue). In comparison to literature studies, where quenching rates >90% were observed, the values found in our study are comparably low. This is predominantly attributed to the fact that the Alq_3 was not fixed on the NP surface and that unbound dye molecules were not removed in this experimental setup. Nonetheless, a significantly more pronounced quenching was found for the dispersed particles in comparison to the aggregated ones. This may be due to the more intensive overlap between the SPR maximum of the particles and the dye's emission spectrum, which could enhance the non-radiative quenching rate. These experimental results could indicate that the plasmonic state of the redispersed AuNPs turned back to that of the initial state of the dispersed AuNPs. However, it should be noted that next to the plasmonic state, the total surface area of the AuNP also significantly increased in comparison to the agglomerated particles. Consequently, the higher abundance of surface area could lead to a higher number of binding events of the dye molecules to the metal surface, which could also result in a more pronounced quenching.

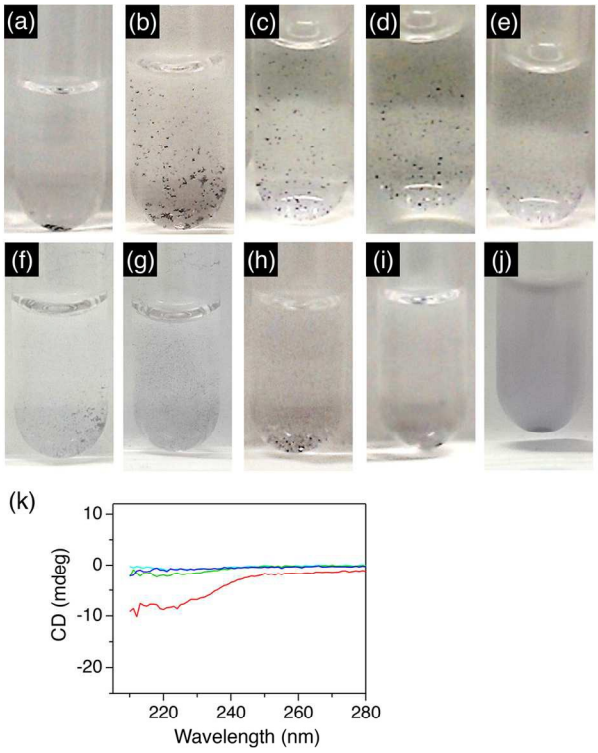

Fig. 4. Photographs of aqueous dispersions of agglomerated AuNPs after addition of MeOH solutions of H-VKVVC (a), Fmoc-KVVC (b), Fmoc-VVC (c), Fmoc-VC (d), Fmoc-KC (e), Fmoc-VVVKC (f), Fmoc-VVVVC (g), Fmoc-VKVVE (h), Fmoc-VKVVH (i) and 1-dodecanethiol (j). (k) CD spectra of MeOH solutions of Fmoc-KVVC (red), Fmoc-VVC (blue), Fmoc-VC (green), and Fmoc-KC (light blue).

When the concentration of the added peptide solution was increased by two or three times, the incubation time required for the redispersion of agglomerated AuNPs is shortened to 1–2 days. On the other hand, when the concentration of the added peptide was reduced, a clear threshold for the redispersion of agglomerated AuNPs was observed. Figure 2g shows the absorbance change upon addition of Fmoc-VKVVC in MeOH to the aqueous solution of agglomerated AuNPs. Less than 0.0625 mM of the total concentration of Fmoc-VKVVC resulted in much heavier agglomeration, leading to the decrease of the absorbance of AuNPs. This is probably attributed to the well-known charge compensation effect, previously described by Gamrad *et al.* for negatively-charged nanoparticles and positively-charged peptides.[9g] At a certain concentration regime, an isoelectric point is reached where charge compensation induces impairment of the colloidal stability. This tendency is similar to the aggregation of AuNPs when cysteine was added to aqueous dispersion of AuNPs.[18] In contrast, when the total concentrations of Fmoc-VKVVC were increased to 0.125 and 0.25 mM, the absorbance of AuNPs at 530 nm was increased (Fig. 2g, inset). CD spectra of Fmoc-VKVVC also show concentration dependency, where the concentration of Fmoc-VKVVC higher than 0.125 mM displays negative ellipticity at 210 nm, while that less than 0.0625 mM shows negligible ellipticity at that wavelength region (Fig. 2h). These spectroscopic results clearly indicate that the β-sheet

Table 1. Secondary Structure in MeOH (0.5 mM) and Dispersion Properties of Agglomerated MNPs

Sequence & Structure	Assembly in MeOH	Dispersion Property[1]
Fmoc-VKVVC	β-Sheet	○
H-VKVVC	Random	×
Fmoc-KVVC	Random	×
Fmoc-VVC	Random	×
Fmoc-VC	Random	×
Fmoc-C	Random	×
Fmoc-KC	Random	×
Fmoc-VVVKC	Random	×
Fmoc-VVVVC	Insoluble	×
Fmoc-VKVVE	β-Sheet[2]	×
Fmoc-VKVVH	Random	×
1-dodecanethiol	Soluble	×

[1] ○; well-dispersive, ×; hardly dispersive. [2] Reference 7c.

formation of Fmoc-VKVVC is essential for the redispersion of agglomerated AuNPs.

As a control, addition of Fmoc-C in MeOH to the agglomerated AuNP aqueous dispersion hardly showed the spectral change (Fig. 2e, green).[18] Furthermore,, the addition of MeOH to freshly-prepared AuNPs in water did not result in siginificant changes in the absorption spectra. Therefore, we conclude that the redispersion phenomena are solely related to Fmoc-VKVVC.

We further investigated redispersion properties of Fmoc-VKVVC to other agglomerated MNPs (M = Cu, Pt and Pd). Before addition of the MeOH solution of Fmoc-VKVVC, the MNPs, were heavily agglomerated (Fig. 3, i). By addition of MeOH only or MeOH solution of Fmoc-C, the agglomeration of MNPs intensified, and precipitation could be observed by eyes (Fig. 3, ii and iii). In contrast, by addition of MeOH solutions of Fmoc-VKVVC, the precipitates were readily dispersed by a gentle stirring, and the mixed solutions became homogeneously coloured with high transparency (Fig. 3, iv).

3.4. Influence of secondary structure and amino acid sequences for redispersing MNPs

We systematically investigated which structural components in Fmoc-VKVVC are essential for the dispersion of agglomerated MNPs. First, MeOH solution of H-VKVVC, deprotected form of Fmoc-VKVVC, was added to the aqueous dispersion of agglomerated AuNPs. Here, redispersion of MNPs was hardly observed (Fig. 4a). Next, the number of amino acid residue in Fmoc-VKVVC was reduced one by one from the N-terminus, and the MeOH solutions of Fmoc-peptides (Fmoc-KVVC, Fmoc-VVC, Fmoc-VC) were added to the agglomerated AuNP aqueous dispersion. In all cases, however, redispersion effects were not observed (Fig. 4b–d). Furthermore, Fmoc-KC, without V residues, hardly redispersed the agglomerated AuNPs (Fig. 4e). According to CD spectroscopy, these peptides did not form β-sheet structures in MeOH (Fig. 4k). Therefore, these experiments conclusively confirm that the formation of β-sheet structures is a necessary prerequisite for the redispersion of agglomerated AuNPs.

We further checked redispersion properties of Fmoc-pentapeptides with different amino acid sequences, Fmoc-VVVKC and Fmoc-VVVVC. Fmoc-VVVKC did not form β-sheet in MeOH, which hardly redispersed the agglomerated AuNPs (Fig. 4f). Fmoc-VVVVC itself was hardly dissolved in MeOH and formed a macroscopic precipitation, thus the dispersion of AuNPs became much worse by adding the MeOH suspension containing Fmoc-VVVVC (Fig. 4g).

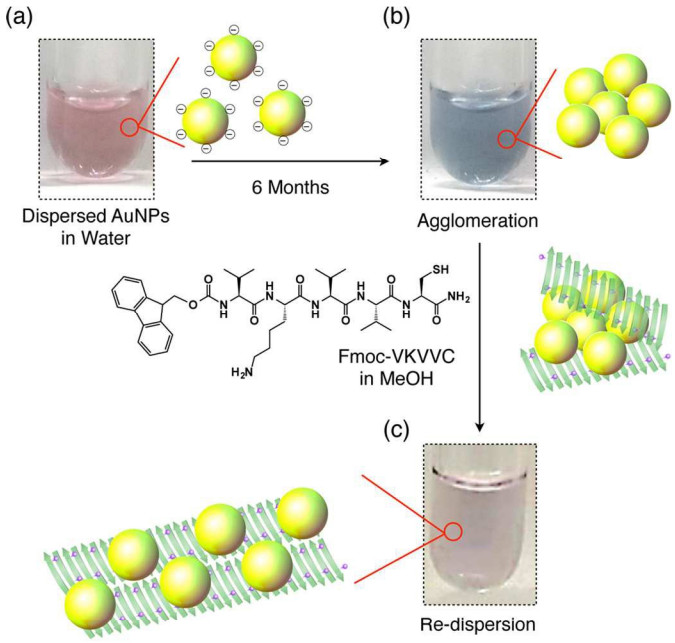

Fig. 5. Schematic representation of the redispersion of MNPs by an addition of Fmoc-VKVVC (β-sheet) in MeOH. Photographs in (a–c) show as-prepared AuNP dispersion in water (a), AuNP dispersion in water 6 months after preparation (b) and that added by MeOH solution of Fmoc-VKVVC aged for 3 days (c). Yellow sphere, green arrow and purple sphere on the green arrow indicate AuNP, β-strand of Fmoc-VKVVC and thiol side chain, respectively.

For comparison, MeOH solutions of Fmoc-VKVVE[9c] and Fmoc-VKVVH, which contain E (negatively charged residue) or H (metal-ion binding residue) instead of C (metal-binding residue), were added to the agglomerated AuNP dispersion. Fmoc-VKVVE formed β-sheet structure in MeOH,[9c] while Fmoc-VKVVH hardly formed β-sheet. Both of these Fmoc-peptides in MeOH did not redisperse agglomerated AuNPs (Fig. 4h and i). Accordingly, metal-binding C seems to be one of the critical structural components for redispersing agglomerated MNPs. We also investigated the redispersion properties in the presence of the non-peptide compound 1-dodecanethiol, including a metal-binding thiol group. However, the AuNPs in water agglomerated much heavier by the addition of MeOH solution of 1-dodecanethiol, however these effects were probably increased by the poor solubility of 1-dodecanethiol in aqueous environments. (Fig. 4j).

4. Discussion

Table 1 summarizes dispersion abilities of the synthesized peptides and 1-dodecanethiol for agglomerated MNPs, along with the secondary structures in MeOH. Only Fmoc-VKVVC disperses agglomerated MNPs efficiently. Fmoc-pentapeptides without cysteine residue hardly disperse agglomerated MNPs.

The role of the Fmoc group is considered to accelerate β-sheet formation via π-π interaction of the fluorenyl moieties.[11] On the other hand, the shorter Fmoc-peptides, Fmoc-KVVC, Fmoc-VVC, Fmoc-VC and Fmoc-KC, as well as Fmoc-amino acid, Fmoc-C, hardly disperse the agglomerated MNPs.[18] Non-peptide compound such as 1-dodecanethiol hardly exhibited re-dispersive property of AuNPs as well.

Figure 5 shows schematic representation of possible mechanism of how the β-sheet redisperses the agglomerated MNPs. β-Sheets of Fmoc-VKVVC possess highly integrated thiol groups on one side. When the MeOH solution of the β-sheet was added to the dispersion of the agglomerated MNPs, the β-sheet subsequently enwraps the MNPs (Fig. 5b). Dissociation of the agglomerated MNPs possibly takes place in the equilibrium of association (β-sheet formation)/dissociation process of Fmoc-VKVVC in solution. Once the MNPs are dissociated, they will be bound on one side of the β-sheet (Fig. 5c). The β-sheet of Fmoc-VKVVC is dispersive in aqueous solution because of the positive charges of K on the other side of the β-sheet, resulting in the highly dispersed MNPs as hybrid. In contrast, Fmoc-VVVKC hardly redispersed agglomerated MNPs possibly because of the lack of the β-sheet secondary structure.

5. Conclusions

In this study, we found that a fluorenyl methoxycarbonyl (Fmoc)-substituted pentapeptide comprising cysteine, lysine and valine has dispersive property for agglomerated ligand-free metal nanoparticles (MNPs, M = Au, Cu, Pt and Pd). Due to the potent assembling feature of Fmoc groups, the Fmoc-pentapeptide adopts β-sheet conformation in MeOH, thus thiol and amino groups of cysteine and lysine, respectively, protrude and integrate separately on the upper and lower sides of β-sheet. When the β-sheets in MeOH were added to the dispersion of the agglomerated MNPs and kept for several days, the colour of the dispersion turned back to the initial state of the highly dispersed MNPs. This behaviour indicates that the plasmonic state is recovered to that of the as-prepared dispersed AuNPs. Systematic studies using various peptides and its concentration dependency clarified that β-sheet formation of the Fmoc-peptide is essential for the redispersion of the agglomerated MNPs. A possible redispersion mechanism is probably attributed to the fact that the agglomerated MNPs are subsequently enwrapped by the β-sheets and gradually separated. Flexible and dispersive β-sheets play an important role for the redispersion of the agglomerated MNPs, in which reconstruction of the β-sheet structure, accompanied by the association/dissociation equilibrium of the Fmoc-pentapeptides, most likely separates off each MNP. Redispersion of the agglomerated MNPs will be useful in the ecological aspect for reusing degenerated MNPs as renewable materials.

Acknowledgements

The authors thank Prof. Kentaro Shiraki and Mr. Shunsuke Yoshizawa of University of Tsukuba for help of PL measurements. This work was partly supported by KAKENHI (25107507, 15H00860 and 15K13812) JSPS/MEXT Japan, Asahi Glass Foundation and German Academic Exchange Service (DAAD)-Tsukuba partnership program. PW and GM gratefully acknowledge funding by German Ministry of Research and Education (BMBF, FKZ 03X5523).

Notes and references

[a] Division of Materials Science, Faculty of Pure and Applied Sciences, University of Tsukuba, 1-1-1 Tennodai, Tsukuba, Ibaraki 305-8573, Japan.
[b] Technical Chemistry I and Center for Nanointegration Duisburg-Essen (CENIDE), University of Duisburg-Essen, NanoEnergieTechnikZentrum (NETZ), Carl-Benz-Strasse 199, 47057 Duisburg, Germany.
[c] Division of Applied Physics, Faculty of Pure and Applied Sciences, University of Tsukuba, 1-1-1 Tennodai, Tsukuba, Ibaraki 305-8573, Japan.
[d] Tsukuba Research Center for Interdisciplinary Materials Science (TIMS), Faculty of Pure and Applied Sciences, University of Tsukuba, 1-1-1 Tennodai, Tsukuba, Ibaraki 305-8573, Japan.
[e] National Institute of Advanced Industrial Science and Technology (AIST), 1-1-1 Higashi, Tsukuba, Ibaraki 305-8566, Japan.

1 (a) M. Haruta, *Chem. Rec*. 2003, **3**, 75; (b) M.-C. Daniel, D. Astruc, *Chem. Rev*. 2004, **104**, 293; (c) E. Yoo, T. Okata, T. Akita, M. Kohyama, J. Nakamura, I. Honma, *Nano Lett*. 2009, **9**, 2255; (d) I. X. Green, W. Tang, M. Neurock, J. T. Yates Jr., *Science* 2011, **333**, 736; (e) H. Yoshida, Y. Kuwauchi, J. R. Jinschek, K. Sun, S. Tanaka, M. Kohyama, S. Shimada, M. Haruta, S. Takeda, *Science* 2012, **335**, 317; (f) K. Ueno, H. Misawa, *NPG Asia Mater*. 2013, **5**, e61; (g) F. Pincella, K. Isozaki, K. Miki, *Light: Sci. Appl.* 2014, **3**, e133.

2 (a) J. H. Lee, J. H. Park, J. S. Kim, D. Y. Lee, K. Cho, *Org. Electr*. 2009, **10**, 416; (b) F.-C. Chen, J.-L. Wu, C.-L. Lee, Y. Hong, C.-H. Kuo, M. H. Huang, *Appl. Phys. Lett*. 2009, **95**, 013305; (c) J.-L. Wu, F.-C. Chen, Y.-S. Hsiao, F.-C. Chien, P. Chen, C.-H. Kuo, M. H. Huang, C.-S. Hsu, *ACS Nano* 2011, **2**, 959; (d) Y. Takahashi, T. Tatsuma, *Appl. Phys. Lett*. 2011, **99**, 182110; (e) X. Li, W. C. Choy, H. Lu, W. E. I. Sha, A. H. P. Ho, *Adv. Funct. Mater*. 2013, **23**, 2728; (f) S.-W. Baek, J. Noh, S.-H. Lee, B. Kim, M.-K. Seo, J.-Y. Lee, *Sci. Rep*. 2013, **3**, 1726; (g) T. Sasaki, K. Tabata, K. Tsukagoshi, A. Beckel, A. Lorke, Y. Yamamoto, *Thin Solid Films* 2014, **562**, 467.

3 J. N. Anker, W. P. Hall, O. Lyandes, N. C. Shah, J. Zhao, R. P. van Duyne, *Nature Mater.* 2008, **7**, 442.

4 (a) F. E. Kruis, H. Fissan, A. Peled, *J. Aerosol. Sci*. 1998, **29**, 511; (b) P. Raveendran, J. Fu, S. L. Wallen, *J. Am. Chem. Soc*. 2003, **125**, 13940; (c) T. K. Sau, C. J. Murphy, *J. Am. Chem. Soc*. 2004, **126**, 8648; (d) W.-H. Chiang, R. M. Sankaran, *Appl. Phys. Lett*. 2007, **91**, 121503; (e) M. Faraji, Y. Yamini, A. Saleh, M. Rezaee, M. Ghambarian, R. Hassani, *Anal. Chim. Acta* 2010, **659**, 172.

5 (a) W. J. Stark, *Angew. Chem. Int. Ed*. 2012, **50**, 1242; (b) M. C. Buford, R. F. Hamilton, A. Holian, *Part. Fibre Toxicol.* 2007, **4,** 6.

6 (a) L. K. Limbach, Y. Li, R. N. Grass, T. J. Brunner, M. A. Hintermann, M. Muller, D. Gunther, W. J. Stark, *Environ. Sci. Technol*. 2005, **39**, 9370; (b) U. Taylor, C. Rehbock, C. Streich, D. Rath S. Barcikowski, *Nanomedicine* 2014, **9**, 1971; (c) L. Foucaud, M. R. Wilson, D. M. Brown, V. Stone, *Toxicol. Lett.* 2007, **174**, 1.

7 F. Maillard, S. Schreier, M. Hanzlik, E. R. Savinova, S. Weinkauf U. Stimming, *Phys. Chem. Chem*. Phys. 2005, **7**, 385.

8 V. Amendola, M. Meneghetti, *Phys. Chem. Chem. Phys.* 2009, **11**, 3805.

9 (a) S. Petersen, A. Barchanski, U. Taylor, S. Klein, D. Rath, S. Barcikowski, *J. Phys. Chem. C* 2011, **115**, 5152; (b) S. Ibrahimkutty, P. Wagener, A. Menzel, A. Plech, S. Barcikowski, *Appl. Phys. Lett*. 2012, **101**, 103104; (c) P. Nachev, D. D. van't Zand, V. Coger, P. Wagener, K. Reimer, P. M. Vogt, S. Barcikowski, A. Pich, *J. Laser Appl.* 2012, **24**, 042012; (d) C. Rehbock, V. Merk, L. Gamrad, R. Streubel, S. Barcikowski, *Phys. Chem. Chem. Phys*. 2013, **15**, 3057; (e) M. Lau, I. Haxhiaj, P. Wagener, R. Intartaglia, F. Brandi, J. Nakamura, S. Barcikowski, *Chem. Phys. Lett.* 2014, **610-611**, 256; (f) G. Marzun, C. Streich, S. Jendrej, S. Barcikowski, P. Wagener, *Langmuir* 2014, **30**, 11928; (g) L. Gamrad, C. Rehbock, J. Krawinkel, B. Tumursukh, A. Heisterkamp, S. Barcikowski, *J. Phys. Chem. C* 2014, **118**, 10302; (h) V. Merk, C. Rehbock, F. Becker, U. Hagemann, H. Nienhaus, S. Barcikowski, *Langmuir* 2014, **30**, 4213; (i) C. Rehbock, J. Jakobi, L. Gamrad, S. van der Meer, D. Tiedemann, U. Taylor, W. Kues, D. Rath S. Barcikowski, Beilstein, *J. Nanotechnol*. 2014, **5**, 1523; (j) G. Marzun, J. Nakamura, X. Zhang, S. Barcikowski, P. Wagener, *Appl. Surface Sci*. 2015, **348**, 75.

10 F. McKenzie, K. Faulds, D, Graham, *Chem. Commun*. 2008, 2367.

11 (a) P. Vairaprakash, H. Ueki, K. Tashiro, O. M. Yaghi, *J. Am. Chem. Soc*. 2011, **133**, 759; (b); A. M. Fracaroli, K. Tashiro, O. M. Yaghi, *Inorg. Chem*. 2012, **51**, 6437; (c) T. Nakayama, T. Sakuraba, S. Tomita, A. Kaneko, E. Takai, K. Shiraki, K. Tashiro, N. Ishii, Y. Hasegawa, Y. Yamada, R. Kumai, Y. Yamamoto, *Asian J. Org. Chem*. 2014, **3**, 1182.

12 A.-M. Fernandez-Escamilla, F. Rousseau, J. Schmkowitz, L. Serrano, *Nature Biotechnol*. 2004, **22**, 1302.

13 E. L. Bakota, O. Sensoy, B. Ozgur, M. Sayar, J. D. Hartgerink, *Biomacromolecules* 2013, **14**, 1370.

14 C. J. Bowerman, B. L. Nilson, *Pept. Sci*. 2012, **98**, 169.

15 (a) Z. Yang, H. Gu, D. Fu, P. Gao, J. K. Lam, B. Xu, *Adv. Mater.* 2004, **16**, 1440; (b) Z. Yang, H. Gu, Y. Zhang, L. Wang, B. Xu, *Chem. Commun*. 2004, 208; (c) A. Mahler, M. Reches, M. Rechter, S. Cohen, E. Gazit, *Adv. Mater*. 2006, **18**, 1365; (d) A. R. Hirst, S. Roy, M. Arora, A. K. Das, N. Hodson, P. Murray, S. Marshall, N. Javid, J. Sefcik, J. Boekhoven, J. H. van Esch, S. Santabarbara, N. T. Hunt, R. V. Ulijn, *Nature Chem*. 2010, **2**, 1089.

16 (a) C. Fan, S. Wang, J. W. Hong, G. C. Bazan, K. W. Plaxco, A. J. Heeger, *Proc. Natl. Acad. Sci. USA*, 2003, **100**, 6297; (b) U. S. Raikar, V. B. Tangod, B. M. Mastiholi, V. J. Fulari, *Opt. Commun*. 2011, **284**, 4761; (c) R. Schreiber, J. Do, E.-M. Roller, T. Zhang, V. J. Schüller, P. C. Nickels, J. Feldmann, T. Liedl, *Nature Nanotechnol*. 2014, **9**, 74; (d) D. Ghosh and N. Chattopadhyay, *J. Luminescence* 2015, **160**, 223.

17 (a) E. Dulkeith, A. C. Morteani, T. Niedereichholz, T. A. Klar, J. Feldmann, S. A. Levi, F. van Veggel, D. N. Reinhoudt, M. Möller, D. I. Gittins, *Phys. Rev. Lett.* 2002, **89**, 203002; (b) E. Dulkeith, M. Ringler, T. A. Klar, J. Feldmann, *Nano Lett*. 2005, **5**, 585.

18 R. G. Acres, V. Feyer, N. Tsud, E. Carlino, K. C. Prince, *J. Phys. Chem. C* 2014, **118**, 10481.

